

SCIENTIFIC DATA

OPEN

SUBJECT CATEGORIES

- » Biological physics
- » Virus structures
- » X-rays

Received: 04 February 2016

Accepted: 22 June 2016

Published: 1 August 2016

Data Descriptor: Single-shot diffraction data from the Mimivirus particle using an X-ray free-electron laser

Tomas Ekeberg *et al.*[#]

Free-electron lasers (FEL) hold the potential to revolutionize structural biology by producing X-ray pulses short enough to outrun radiation damage, thus allowing imaging of biological samples without the limitation from radiation damage. Thus, a major part of the scientific case for the first FELs was three-dimensional (3D) reconstruction of non-crystalline biological objects. In a recent publication we demonstrated the first 3D reconstruction of a biological object from an X-ray FEL using this technique. The sample was the giant Mimivirus, which is one of the largest known viruses with a diameter of 450 nm. Here we present the dataset used for this successful reconstruction. Data-analysis methods for single-particle imaging at FELs are undergoing heavy development but data collection relies on very limited time available through a highly competitive proposal process. This dataset provides experimental data to the entire community and could boost algorithm development and provide a benchmark dataset for new algorithms.

Design Type(s)	macromolecular structure generation objective
Measurement Type(s)	X-ray diffraction data
Technology Type(s)	X-ray free electron laser
Factor Type(s)	
Sample Characteristic(s)	Acanthamoeba polyphaga mimivirus

Correspondence and requests for materials should be addressed to T.E. (email: ekeberg@xray.bmc.uu.se).
[#]A full list of authors and their affiliations appears at the end of the paper.

Background & Summary

Free-electron lasers (FEL) provide ultra short and extremely bright pulses of coherent X-rays¹. It has been predicted that such pulses could enable structure determination without crystallization by outrunning radiation damage and thus capturing diffraction data before the particle has time to respond and eventually be destroyed by the deposited energy². Experimental verification of this 'diffraction-before-destruction' principle has been demonstrated several times for resolution down to 10 nm (refs 3,4).

Using many such diffraction patterns from multiple copies of a reproducible sample, the patterns could be assembled into a 3D diffraction space from which the 3D structure could be derived^{5,6}. This promise was a main part of the scientific case for building free-electron lasers⁷. Several examples of 2D reconstructions from biological samples at X-ray FEL have been demonstrated^{4,8,9} but 3D reconstructions have remained elusive.

A single diffraction pattern represents a curved slice through the Fourier transform of the electron density of the object. For successful 3D reconstruction many diffraction patterns from identical particles need to be assembled into the complete 3D Fourier transform of the particle. This is difficult since the orientation of the injected particles is unknown and has to be recovered from the diffraction data alone. A recent paper¹⁰ demonstrates this, using a modified version of the expand, maximize and compress algorithm⁵ (EMC) on the Mimivirus particle. Here we describe the data collection, data preprocessing and the dataset that was used for this reconstruction.

Today, beam time at free-electron lasers is scarce as there are few facilities and they serve a multitude of scientific disciplines. Furthermore, applications such as 3D imaging require a large amount of effort in algorithm development and testing. Several groups around the world are active in this development but the majority of them don't have regular beam time access. This dataset can thus serve as a benchmark for algorithm testing and give many more groups access to experimental data.

For any new method, validation tools are of crucial importance. Therefore, together with the 3D reconstruction of the Mimivirus we also presented two new validation methods¹⁰. Further development of these methods, and the development of new ones will therefore benefit from being applied to this dataset in particular.

The sample in this dataset is the Mimivirus (*Acanthamoeba polyphaga mimivirus*)^{11,12}. Mimivirus is part of a recently discovered class of giant DNA viruses. Viral capsid is pseudo-icosahedral with a corner-to-corner diameter of 500 nm and a face-to-face diameter of 400 nm (ref. 13). The virus is covered by fibres with a length of 125 nm giving it a total diameter of 750 nm (ref. 14).

Methods

These methods were described in ref. 10. The description here is more detailed with regards to data collection and on-line data analysis.

Sample injection

Purified Mimivirus particles¹⁵ were transferred into a volatile buffer (250 mM ammonium acetate, pH 7.5) and the suspension was aerosolized with helium in a gas dynamic nebulizer¹⁶. The aerosol of hydrated and adiabatically cooled particles entered a differentially pumped aerodynamic lens¹⁷.

Data collection

Experiments were performed at the Atomic Molecular Optics (AMO) beam line¹⁸ of the Linac Coherent Light Source (LCLS) hard X-ray laser¹, using the CAMP¹⁹ instrument^{20,21}. The experiment was part of an experiment running from June 17 to June 21 of 2010 with proposal number L150. Diffraction data were recorded on a pair of pnCCD detectors¹⁹ at a repetition rate of 60 Hz matching the repetition rate of LCLS. The two detectors were placed at a distance of 740 mm from the interaction region with a gap between them of 2.1 mm to let the direct beam through. The pixel size is 75 μm and each detector in the pair has $512 \times 1,024$ pixels giving the full setup a pixel count of $1,024 \times 1,024$ pixels.

The photon energy was 1.2 keV corresponding to a wavelength of 1.03 nm. At this wavelength the full-period resolution at the edge of the detector is 19.9 nm. The electron bunch used to create the X-ray pulse was 70 fs long (full duration at half maximum) and the X-ray pulse is believed to be shorter than this²². The focus was $\sim 10 \mu\text{m}$ (full width at half maximum) at the interaction point, giving a power density of $\sim 3.4 \cdot 10^{15} \text{ W cm}^{-2}$ or 10^{12} photons per pulse.

The experiment was performed at a pressure of 10^{-6} mbar to reduce background scattering. Some of the most important experiment parameters are summarized in Table 1.

On-line data analysis

On-line hit-identification provided real-time statistics that guided injector alignment and tuning. Hits with a high scattering strength were identified by counting the number of pixels that measured a value above a threshold. Diffraction patterns with more than 500 pixels with a value above 170 ADU were defined as a hit. See ref. 21 for a detailed description.

Data Records

Two datasets are provided: the full record of all collected data and a smaller preprocessed dataset. Both data sets are available in the same CXIDB entry (Data Citation 1).

Parameter	Value
Photon energy	1,200 keV
Detector distance	0.74 m
Pixel size	75 μm
Number of pixels	1,024 \times 1,024
Focal size	10 μm^2

Table 1. Summary of experimental parameters.

Run number	Sample	Number of frames	Number of frames selected for analysis in ref. 10
73	Dark	651	N/A
80	Mimivirus	14,273	0
81	Mimivirus	14,450	0
82	Mimivirus	11,371	0
83	Dark	15,636	N/A
84	Mimivirus	65,594	0
87	Mimivirus	93,840	0
89	Dark	3,821	N/A
90	Mimivirus	77,644	30
91	Mimivirus	4,943	6
92	Mimivirus	33,721	39
93	Mimivirus	43,679	24
94	Mimivirus	58,931	40
95	Mimivirus	42,083	10
97	Mimivirus	36,899	33
98	Dark	7,794	N/A
152	Dark	2,498	N/A
156	Mimivirus	64,977	3
157	Mimivirus	90,403	13

Table 2. List of experimental runs. Runs labeled as dark had the X-ray beam turned off and are included to allow for detector calibration. The lack of good hits before run 90 was possibly fixed by a changed injection nozzle at this point.

Full data record

We provide all data collected from the Mimivirus at this beamtime before any preprocessing or sorting. This dataset is in the extended tagged container (XTC) file format. This can be converted to HDF5 format using programs such as CASS²³ or Cheetah²⁴. This conversion normally also involves preprocessing and the data is therefore provided in the untouched XTC format.

The record contains 19 LCLS runs. 14 of these had the sample injector and X-ray laser turned on while the remaining 5 runs only collected detector background noise. These so called ‘dark runs’ can be used for to better subtract the background from the actual data. Table 2 shows a list of all 19 runs.

Initial hit finding showed that 0.3% of the frames contained diffraction that was stronger than the background. The rest were misses, i.e., frames that were read out when the pulse did not hit any particle. In addition to hits from single Mimivirus particles the hits also include droplets of buffer, clusters of viruses and a few particles that were injected earlier and had stayed in the injection system.

Preprocessed and filtered data

This dataset contains the 198 preprocessed (see ref. 19) diffraction patterns that were used in ref. 10 to recover the 3D structure of the Mimivirus particle. This data is in the CXIDB format described in ref. 25. The pixel values in the data are in arbitrary detector units (ADU). The conversion factor from ADU to number of photons is 7 ADU per photon. Some areas of the detector were unreadable and some scattering angles were not covered by the detector, such as the gap between the two detector halves that lets the direct beam through. These areas are identified by a *mask* entry in the CXIDB file format.

The data was filtered in three steps. (1) Hits were distinguished from blanks using methods described in refs 21 and 24. This yielded 1,600 hits. (2) 307 Diffraction patterns that correspond to a Mimivirus

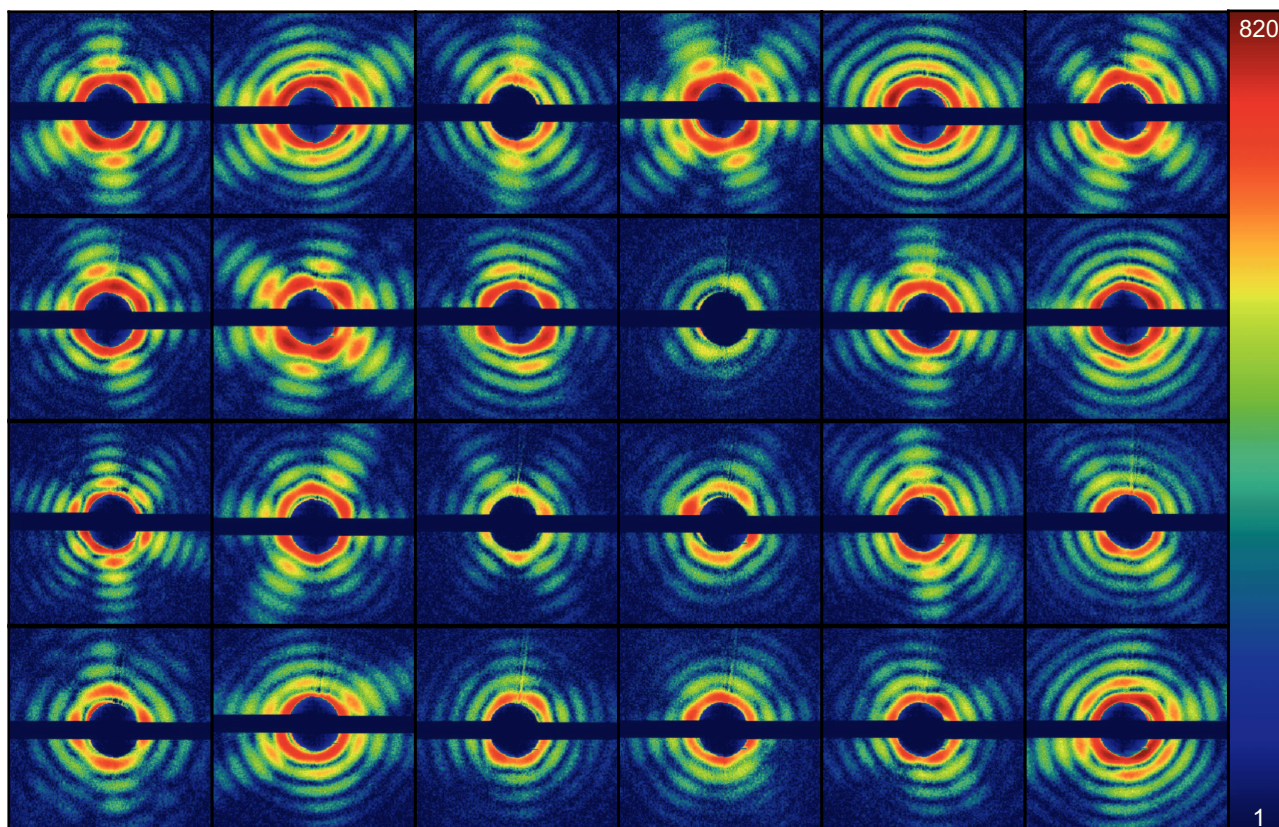


Figure 1. The first 24 of the 198 diffraction patterns in this dataset. The color scale is logarithmic and ranges from 1 to 820 photons per pixel. This is a modification of a figure previously presented in ref. 10.

particle were selected by hand. An icosahedral or pseudo-icosahedral particle will in most orientations yield a distinctive type of pattern showing six outwards-going streaks. This feature and particle size, determined from the fringe spacing, was used for this selection. (3) When the detector is exposed to high intensities, the intensity can spill over from a pixel to neighboring pixels. We start seeing these effects at intensities above 750 photons per pixel. In the final dataset, diffraction patterns suffering from this effect were filtered out, resulting in 198 unsaturated diffraction patterns. A subset of this dataset is shown in Fig. 1.

Technical Validation

3D reconstruction

The 198 diffraction patterns were successfully assembled in a 3D Fourier volume and subsequent phase retrieval provided the full 3D electron density of the virus with a full-period resolution of 125 nm¹⁰. This indicates that the Mimivirus is reproducible to at least this resolution.

Validation of the 3D reconstruction

In cryo-electron microscopy (cryo-EM), data is routinely split prior to analysis and the analysis is performed in parallel on the two sets²⁶. Our first method for validating the 3D reconstruction is an adaptation of this technique. The diffraction patterns are randomly split in two sets of equal size. The recovery of the 3D alignment is performed independently on the two sets using the same parameters but independent random starting points. Phase retrieval is also performed independently using the same parameters. The standard practice in the field is to repeat the reconstruction at least 100 times and the results are then averaged to average out effects of the random starting point^{4,27}.

The EMC algorithm recovers the relative orientation of the particles from the diffracted data alone but the arbitrary rotation of the entire system can be different comparing the two resulting 3D electron density maps. In order to compare the two recovered electron densities we therefore have to rotate one of the two data sets to best match the other. This is done using brute force by interpolating one of the maps at a regular array corresponding to the tested rotation. To compare the two maps, the Pearson correlation coefficient is calculated. The rotation with the highest Pearson correlation is assumed to correspond to the proper relative orientation.

The two aligned electron density maps are then compared using the Fourier shell correlation (FSC)²⁶, which provides a measure of the similarity as a function of resolution. The threshold for what is regarded as an acceptable fit ranges between 0.14 and 0.5 in cryo-EM literature^{28,29}.

In X-ray crystallography some Bragg spots are usually excluded from the analysis and instead that information is used to verify the recovered expected strength of the respective Bragg spot³⁰. Using the same idea, 10% of the diffraction patterns were selected to be used for validation only. In the EMC scheme these patterns are excluded from the analysis but are still compared to the recovered Fourier transform of the particle. The measure for determining whether the recovered model agrees with the excluded diffraction patterns is the likelihood function used internally in EMC.

The analogy with the R_{free} value in crystallography should not be over emphasized. Bragg peaks are linearly independent parameters and there is no suitable analogy in the continuous diffraction case. Furthermore, in the case described here, the process that is validated is that of pattern alignment and not phase retrieval. It is therefore natural to choose individual diffraction patterns as the information unit to exclude rather than i.e., individual pixels or regions of pixels.

These validation methods were previously described in ref. 10.

Usage Notes

Data was stored in the CXIDB²⁵ data format which uses the HDF5 format. HDF5 files are readable in many computing environments including python using the h5py module and MATLAB using e.g., the h5read function. Convenient functions for accessing the CXIDB data file exist in the libspimage package for C and python³¹. For visualizing data the CXIDB file browser Owl (<https://github.com/FilipeMaia/owl>) is recommended.

References

1. Emma, P. *et al.* First lasing and operation of an ångström-wavelength free-electron laser. *Nat. Photonics* **4**, 641–647 (2010).
2. Neutze, R., Wouts, R., van der Spoel, D., Weckert, E. & Hajdu, J. Potential for biomolecular imaging with femtosecond X-ray pulses. *Nature* **406**, 752–757 (2000).
3. Chapman, H. N. *et al.* Femtosecond diffractive imaging with a soft-X-ray free-electron laser. *Nat. Phys.* **2**, 839–843 (2006).
4. Seibert, M. M. *et al.* Single mimivirus particles intercepted and imaged with an X-ray laser. *Nature* **470**, 78–81 (2011).
5. Loh, N.-T. D. & Elser, V. Reconstruction algorithm for single-particle diffraction imaging experiments. *Phys. Rev. E. Stat. Nonlin. Soft Matter Phys.* **80**, 026705 (2009).
6. Fung, R., Shneerson, V., Saldin, D. K. & Ourmazd, A. Structure from fleeting illumination of faint spinning objects in flight. *Nat. Phys.* **5**, 64–67 (2008).
7. Galayda, J. *LCLS The First Experiments*. Available at <http://www.slac.stanford.edu/pubs/slacreports/reports03/slac-r-611.pdf> (2003).
8. Hantke, M. F. *et al.* High-throughput imaging of heterogeneous cell organelles with an X-ray laser. *Nat. Photonics* **8**, 943–949 (2014).
9. van der Schot, G. *et al.* Imaging single cells in a beam of live cyanobacteria with an X-ray laser. *Nat. Commun.* **6**, 5704 (2015).
10. Ekeberg, T. *et al.* Three-Dimensional Reconstruction of the Giant Mimivirus Particle with an X-Ray Free-Electron Laser. *Phys. Rev. Lett.* **114**, 098102 (2015).
11. Raoult, D. *et al.* The 1.2-megabase genome sequence of Mimivirus. *Science* **306**, 1344–1350 (2004).
12. Claverie, J.-M. & Abergel, C. Mimivirus and its virophage. *Annu. Rev. Genet.* **43**, 49–66 (2009).
13. Xiao, C. *et al.* Structural studies of the giant mimivirus. *PLoS Biol.* **7**, e92 (2009).
14. Xiao, C. *et al.* Cryo-electron microscopy of the giant Mimivirus. *J. Mol. Biol.* **353**, 493–496 (2005).
15. Byrne, D. *et al.* The polyadenylation site of Mimivirus transcripts obeys a stringent 'hairpin rule'. *Genome Res.* **19**, 1233–1242 (2009).
16. DePonte, D. P. *et al.* Gas dynamic virtual nozzle for generation of microscopic droplet streams. *J. Phys. D. Appl. Phys.* **41**, 195505 (2008).
17. Bogan, M., Benner, W. & Boutet, S. Single particle X-ray diffractive imaging. *Nano Lett.* **8**, 310–316 (2008).
18. Bostedt, C. *et al.* Ultra-fast and ultra-intense X-ray sciences: first results from the Linac Coherent Light Source free-electron laser. *J. Phys. B At. Mol. Opt. Phys.* **46**, 164003 (2013).
19. Strüder, L. *et al.* Large-format, high-speed, X-ray pnCCDs combined with electron and ion imaging spectrometers in a multipurpose chamber for experiments at 4th generation light sources. *Nucl. Instruments Methods Phys. Res. Sect. A Accel. Spectrometers, Detect. Assoc. Equip.* **614**, 483–496 (2010).
20. Yoon, C. H. *et al.* Unsupervised classification of single-particle X-ray diffraction snapshots by spectral clustering. *Opt. Express* **19**, 16542 (2011).
21. Kassemeyer, S. *et al.* Femtosecond free-electron laser X-ray diffraction data sets for algorithm development. *Opt. Express* **20**, 4149 (2012).
22. Young, L. *et al.* Femtosecond electronic response of atoms to ultra-intense X-rays. *Nature* **466**, 56–61 (2010).
23. Foucar, L. *et al.* CASS—CFEL-ASG software suite. *Comput. Phys. Commun.* **183**, 2207–2213 (2012).
24. Barty, A. *et al.* Cheetah: software for high-throughput reduction and analysis of serial femtosecond X-ray diffraction data. *J. Appl. Crystallogr.* **47**, 1118–1131 (2014).
25. Maia, F. R. N. C. The Coherent X-ray Imaging Data Bank. *Nat. Methods* **9**, 854–855 (2012).
26. Harauz, G. & van Heel, M. Exact filters for general geometry three dimensional reconstruction. *Optik (Stuttg)* **78**, 146–156 (1986).
27. Chapman, H. N. *et al.* High-resolution ab initio three-dimensional X-ray diffraction microscopy. *J. Opt. Soc. Am. A Opt. Image Sci. Vis.* **23**, 1179–1200 (2006).
28. Rosenthal, P. B. & Henderson, R. Optimal Determination of Particle Orientation, Absolute Hand, and Contrast Loss in Single-particle Electron Cryomicroscopy. *J. Mol. Biol.* **333**, 721–745 (2003).
29. Böttcher, B., Wynne, S. & Crowther, R. Determination of the fold of the core protein of hepatitis B virus by electron cryomicroscopy. *Nature* **386**, 88–91 (1997).
30. Brünger, A. Free R value: a novel statistical quantity for assessing the accuracy of crystal structures. *Nature* **355**, 472 (1992).
31. Maia, F. R. N. C., Ekeberg, T., van der Spoel, D. & Hajdu, J. Hawk: the image reconstruction package for coherent X-ray diffractive imaging. *J. Appl. Crystallogr.* **43**, 1535–1539 (2010).

Data Citation

1. Ekeberg, T. *et al.* *Coherent X-ray Imaging Data Bank* <http://dx.doi.org/10.11577/1236752> (2015).

Acknowledgements

This work was supported by the Swedish Research Council, the Knut and Alice Wallenberg Foundation, the Max Planck Society, the European Research Council, the Röntgen-Ångström Cluster, and Stiftelsen Olle Engkvist Byggmästare. Portions of this research were carried out at the Linac Coherent Light Source, a national user facility operated by Stanford University on behalf of the US Department of Energy, Office of Basic Energy Sciences. We are grateful to the scientific and technical staff of the LCLS for support.

Author Contributions

T.E. wrote the manuscript with contributions from all authors. C.A., J.-M.C., V.S. contributed the Mimivirus particles. D.D.P., R.L.S., L.L., M.J.B. developed and ran the sample delivery system. O.J., D.W., B.I., C.Y.H., R.S., M.S., D.O. prepared the samples and performed offline injection analysis. L.F., S.K. performed the online data analysis. M.M.L., N.-T.D.L., F.R.N.C.M., M.F.H., T.E., A.M., A.B. performed offline data analysis. L.F., S.W.E., D.R., A.R., B.R., B.E., J.U., C.S., F.K., I.S. designed, constructed, and operated the CAMP instrument. R.H., A.H., N.K., P.H., L.S., G.W., G.H., C.R., and H.S. designed, constructed, and operated the pnCCD detectors. C.W., H.H., and H.G. contributed to the detector and its implementation. S.B., M.B., H.F., and L.G. contributed instrumentation. J.K. characterized the FEL focus. A.A., J.A., B.I., M.M., S.S., N.C., C.B., J.D.B., M.F., M.S., and J.A. were involved in collecting the data. C.B. and J.D.B. were in charge of the AMO endstation. I.S., M.B., H.C., and J.H. designed the experiment. I.A. and J.H. conceived the experiment.

Additional Information

Competing financial interests: The authors declare no competing financial interest.

How to cite this article: Ekeberg, T *et al.* Single-shot diffraction data from the Mimivirus particle using an X-ray free-electron laser. *Sci. Data* 3:160060 doi: 10.1038/sdata.2016.60 (2016).



This work is licensed under a Creative Commons Attribution 4.0 International License. The images or other third party material in this article are included in the article's Creative Commons license, unless indicated otherwise in the credit line; if the material is not included under the Creative Commons license, users will need to obtain permission from the license holder to reproduce the material. To view a copy of this license, visit <http://creativecommons.org/licenses/by/4.0>

Metadata associated with this Data Descriptor is available at <http://www.nature.com/sdata/> and is released under the CC0 waiver to maximize reuse.

© The Author(s) 2016

Tomas Ekeberg^{1,2}, Martin Svenda¹, M. Marvin Seibert¹, Chantal Abergel³,
 Filipe R.N.C. Maia¹, Virginie Seltzer³, Daniel P. DePonte^{2,4}, Andrew Aquila^{4,5},
 Jakob Andreasson¹, Bianca Iwan^{1,6}, Olof Jönsson^{1,7}, Daniel Westphal¹, Duško Odić¹,
 Inger Andersson¹, Anton Barty², Meng Liang^{2,4}, Andrew V. Martin^{2,8}, Lars Gumprecht²,
 Holger Fleckenstein², Saša Bajt⁹, Miriam Barthelmess⁹, Nicola Coppola²,
 Jean-Michel Claverie³, N. Duane Loh^{10,11}, Christoph Bostedt⁴, John D. Bozek¹²,
 Jacek Krzywinski⁴, Marc Messerschmidt⁴, Michael J. Bogan¹⁰, Christina Y. Hampton¹⁰,
 Raymond G. Sierra¹⁰, Matthias Frank¹³, Robert L. Shoeman¹⁴, Lukas Lomb¹⁴,
 Lutz Foucar^{14,15}, Sascha W. Epp^{15,16}, Daniel Rolles^{14,15,17}, Artem Rudenko^{15,16,17},
 Robert Hartmann¹⁸, Andreas Hartmann¹⁸, Nils Kimmel^{19,20}, Peter Holl¹⁸,
 Georg Weidenspointner^{19,20}, Benedikt Rudek^{15,16}, Benjamin Erk^{15,16},
 Stephan Kassemeyer¹⁴, Ilme Schlichting^{14,15}, Lothar Strüder^{18,21}, Joachim Ullrich^{15,16,22},
 Carlo Schmidt^{15,16}, Faton Krasniqi^{14,15}, Günter Hauser^{19,20}, Christian Reich¹⁸,
 Heike Soltau¹⁸, Sebastian Schorb²³, Helmut Hirsemann⁹, Cornelia Wunderer⁹,
 Heinz Graafsma⁹, Henry Chapman^{2,24} & Janos Hajdu^{1,5}

¹Department of Cell and Molecular Biology, Laboratory of Molecular Biophysics, Uppsala University, Husargatan 3 (Box 596), SE-751 24 Uppsala, Sweden. ²Center for Free-Electron Laser Science, DESY, Notkestrasse 85, 22607 Hamburg, Germany. ³Information Génomique et Structurale (UMR7256) CNRS & Aix-Marseille Université, Institut de Microbiologie de la Méditerranée (FR3479), Parc Scientifique de Luminy, Case 934, 13288 Marseille Cedex 9, France. ⁴LCLS, SLAC National Accelerator Laboratory, 2575 Sand Hill Road, Menlo Park, California 94025, USA. ⁵European XFEL, Albert-Einstein-Ring 19, 22761 Hamburg, Germany. ⁶Commissariat à l'énergie atomique et aux énergies alternatives, Centre d'études de Saclay, 91191 Gif sur Yvette cedex, France. ⁷Molekyl- och kondenserade materiens fysik, Institutionen för Fysik och Astronomi, Uppsala University, Lägerhyddsvägen 1 (Box 524), SE-751 20 Uppsala, Sweden. ⁸The University of Melbourne, 161 Barry Street, Parkville, 3010 Victoria, Australia. ⁹Photon Science, DESY, Notkestrasse 85, 22607 Hamburg, Germany. ¹⁰Stanford PULSE Institute, SLAC National Accelerator Laboratory, 2575 Sand Hill Road, Menlo Park, California 94025, USA. ¹¹Centre for BioImaging Sciences, National University of Singapore, 14 Science Drive 4 Blk S1 A, Singapore 117546, Singapore. ¹²Synchrotron SOLEIL, L'orme des Merisiers roundabout of St Aubin, 91190 Saint Aubin, France. ¹³Lawrence Livermore National Laboratory, 7000 East Avenue, Mail Stop L-211, Livermore, California 94551, USA. ¹⁴Max-Planck-Institut für medizinische Forschung, Jahnstr. 29, 69120 Heidelberg, Germany. ¹⁵Max Planck Advanced Study Group, Center for Free Electron Laser Science, Notkestrasse 85, 22607 Hamburg, Germany. ¹⁶Max-Planck-Institut für Kernphysik, Saupfercheckweg 1, 69117 Heidelberg, Germany. ¹⁷Department of Physics, J.R. Macdonald Laboratory, Kansas State University, 116 Cardwell Hall, Manhattan, Kansas 66506, USA. ¹⁸PNSensor GmbH, Otto-Hahn-Ring 6, 81739 Munich, Germany. ¹⁹Max-Planck-Institut Halbleiterlabor, Otto-Hahn-Ring 6, 81739 Munich, Germany. ²⁰Max-Planck-Institut für extraterrestrische Physik, Giessenbachstrasse, 85741 Garching, Germany. ²¹Universität Siegen, Emmy-Noether Campus, Walter Flex Str. 3, 57068 Siegen, Germany. ²²Physikalisch-Technische Bundesanstalt, Bundesallee 100, 38116 Braunschweig, Germany. ²³Institut für Optik und Atomare Physik, Technische Universität Berlin, Hardenbergstrasse 36, 10623 Berlin, Germany. ²⁴University of Hamburg, Notkestrasse 85, 22607 Hamburg, Germany.